International Journal of Earth, Energy and Environmental Sciences
ISSN: 2517-942X
Vol:9, No:12, 2015

Theoretical Model of a Flat Plate Solar Collector Integrated with Phase Change Material

Mouna Hamed, Ammar B. Brahim

***Abstract*—**The objective of this work was to develop a theoretical model to study the dynamic thermal behavior of a flat plate solar collector integrated with a phase change material (PCM). The PCM acted as a heat source for the solar system during low intensity solar radiation and night. The energy balance equations for the various components of the collector as well as for the PCM were formulated and numerically solved using Matlab computational program. The effect of natural convection on heat during the melting process was taken into account by using an effective thermal conductivity. The model was used to investigate the effect of inlet water temperature, water mass flow rate, and PCM thickness on the outlet water temperature and the melt fraction during charging and discharging modes. A comparison with a collector without PCM was made. Results showed that charging and discharging processes of PCM have six stages. The adding of PCM caused a decrease in temperature during charge and an increase during discharge. The rise was most enhanced for higher inlet water temperature, PCM thickness and for lower mass flow rate. Analysis indicated that the complete melting time was shorter than the solidification time due to the high heat transfer coefficient during melting. The increases in PCM height and mass flow rate were not linear with the melting and solidification times.

***Keywords*—**Thermal energy storage, phase change material, melting, solidification.

I. Introduction

SOLAR energy plays an important role in replying to the rising demand of energy as well as dealing with pressing climate change and air pollution issues. Its intermittent and dynamic nature makes thermal energy storage systems highly valuable for many solar applications [1], [2]. Latent heat storage using phase change materials (PCM) is one of the most effective methods to store thermal energy due to its high storage density and isothermal behavior during the charging and discharging processes [3]. PCM have been extensively used in practice with an aim to improve the storage capacity of various thermal energy systems. It is possible to use the latent heat of solid-gas, solid-liquid, and liquid-gas transformations; however, only the solid-liquid transformation is used thanks to its lower volume variation [4].

Actually, three different methods to incorporate PCMs into solar thermal system have been suggested: PCM integrated inside the storage tank, the addition of PCM node between the collector and the storage tank and PCM integrated directly in the solar collector [5]. The PCM-integrated solar collector combines collection and storage of thermal energy into a single unit. A system of this type removes the need of conventional storage tanks, thus minimizing space and costs. In recent years, the use of PCMs in solar collector water heater has been developed and analyzed theoretically and experimentally. Tiwari et al. [6] developed a theoretical analysis of PCM storage water heater by incorporating the effect of water flow through a parallel plate placed at the solid-liquid interface. To minimize the night heat loss, the exposed surface was covered by a movable insulation. They proved that during day and night the hot water can be made available at a temperature 15-20°C higher than the ambient temperature, and a rise in the melted region caused a decrease of the water temperature fluctuations. Rabin et al. [7] designed an integrated solar collector storage system with salt hydrate eutectic mixture (48% $CaCl_2$, 4.5% KCl, 0.4% NaCl and 47.1% H_2O) as PCM. They developed a mathematical model for the charging process based on heat conduction and neglected the effect of natural convection. The results showed that the PCM layer plays an important role in the location of the propagation distance of the solid interface of the solid-liquid PCM interface and minor influence on the liquid interface. Kürklü et al. [8] presented a new type of solar collector consisting of two adjoining sections. One section was filled with water and the other with a paraffin wax. They found that the water temperature exceeded 55°C during a typical day of high solar radiation and remained over 36°C during the whole night after the insulation blanket was applied. The energy efficiency values were between about 22% and 80%. Chaabane et al. [9] conducted a numerical study of an integrated collector storage solar water heater with two kinds of PCM (myristic acid and RT-42 graphite) and three radii of this PCM layer. They concluded that the highest water temperature corresponds to the lowest radius unlike the night thermal losses where the optimum case corresponds to the highest radius. Bouadila et al. [10] studied experimentally the thermal performance of an integrated solar latent storage collector with two PCM-filled cavities incorporating below the absorber. The results showed that the paraffin as a PCM contributes to increase the performance of the solar collector at night. Also, they examined numerically the evolution of the PCM melted volume fraction, liquid-solid interfaces, PCM distribution temperature and melting-solidification flow in the PCM-filled cavity.

The purpose of this work is to study the thermal performance of an integrated collector storage solar heater. A mathematical model based on the energy equations was developed. Effects of inlet water temperature, water mass flow

Mouna Hamed and Ammar B. Brahim are with the National Engineering School, University of Gabes, Tunisia (phone: +216 75 392 100; Fax: +216 75 392190; e-mail: Hamedm@hotmail.fr, ammar.benbrahim@enig.rnu.tn).

rate, and PCM thickness were studied and a comparison with a collector without a PCM was made.

II. Description System

The proposed integrated collector storage solar water heater is shown in Fig. 1. It consists of a transparent cover, an air gap, tubes, an absorber, a phase change material, insulations and a container. The solar energy transmitted through the transparent cover is absorbed by the absorber; hence, its temperature increases. Part of thermal energy is transferred by convection to the transfer fluid and the other is transferred by both conduction and convection to the phase change material incorporating below the absorber. When the absorber temperature becomes higher than that of the PCM, heat is first stored as a sensible heat until the PCM reaches its melting temperature. As time elapses, the PCM starts to melt and after complete melting, the heat is stored in the molten PCM as a sensible heat. During low intensity solar radiation periods and night the collector solar components starts to cool down and the PCM acts as a heat source for the flat plate solar system. The PCM releases energy to the absorber and from the latter to the transfer fluid until the PCM completely solidifies.

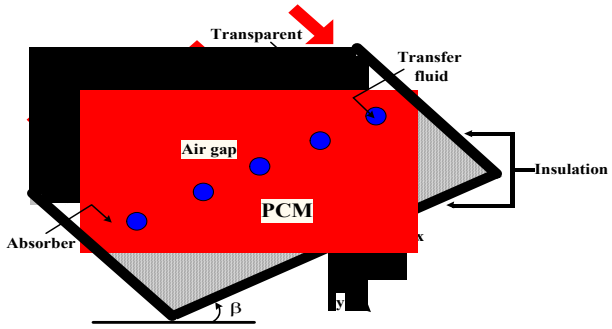

Fig. 1 Schematic of an integrated PCM collector storage solar heater

III. Theoretical Model

This section presents equations for mathematical modeling of the heat transfer processes.

A. Solar Radiation

Global solar radiation absorbed by a tilted collector surface depends upon several variables. Perrin Brinchambaut [11] proposed a theoretical model based on the following correlations. The direct irradiance is calculated as:

$$I = A\cos(\theta_i)\, exp\left(-\frac{1}{B\ \sin(h+2)}\right) \quad (1)$$

where θ_i is the incident angle and h is the sun height.

The diffuse irradiance is given by:

$$D = \left(\frac{1+\cos(\beta)}{2}\right) D_h + \left(\frac{1-\cos(\beta)}{2}\right) \rho\, G_h \quad (2)$$

where β is the tilt angle and ρ is the albedo.

D_h and G_h are expressed as:

$$D_h = A'\left(\sin(h)\right)^{0.4} \quad (3)$$

$$G_h = A''\left(\sin(h)\right)^{B''} \quad (4)$$

B, A', A" and B" are constants which depend on the atmospheric state.

B. Solar Collector

The mathematical model describing the behavior of the integrated collector storage solar water heater is based on the following assumptions:

- The PCM is in perfect contact with the absorber;
- The PCM is homogenous an isotropic;
- The thermo physical properties of the PCM are independent of temperature, but different for solid and liquid phases;
- The PCM behaves ideally, i.e. such phenomena as property degradation and supercooling are not accounted for;
- The PCM is assumed to have a definite melting point.
- No thermal expansion during melting process.
- The heat transfer in the direction of the transfer fluid is ignored.

By writing energy balance equations for all components of the solar collectors: transparent cover, air gap, absorber plate, working fluid and PCM a mathematical model, comprises a set of temperature dependent equations, is obtained.

1. Transparent Cover

$$\begin{aligned} M_C C_C \frac{dT_C}{dt} &= h_{r,C\text{-}sky}\, S_C\left(T_{sky} - T_C\right) + h_{cv,C\text{-}amb} S_C\left(T_{amb} - T_C\right) \\ &+ h_{r,C\text{-}abs}\, S_C\left(T_{abs} - T_C\right) + h_{cv,C\text{-}a}\, S_C\left(T_a - T_C\right) + U_{loss,e} S_{C,e} \\ &.\left(T_{amb} - T_C\right) + \alpha_C S_C G + S_C G \frac{\alpha_C \tau_C \left(1-\alpha_{abs}\right)}{1-\phi_C\left(1-\alpha_{abs}\right)}. \end{aligned} \quad (5)$$

where M, C, T, S, G and α are the mass, the heat capacity, the temperature, the surface, the global solar radiation and the absorption coefficient, respectively. $h_{cv,C\text{-}amb}$ and $h_{cv,C\text{-}a}$ are the heat transfer coefficients by convection, calculated respectively as [12]:

$$h_{cv,C\text{-}amb} = 3.9\ v_{wind} + 5.62 \quad (6)$$

$$h_{cv,C\text{-}a} = \frac{Nu\ \lambda_a}{e_a} \quad (7)$$

v_{wind} is the wind velocity, λ_a is the air thermal conductivity and e_a is the air gap thickness.

The Nusselt number (Nu) is calculated as:

$$Nu = \left(0.06 - 0.017\left(\beta/90\right)\right) Gr^{1/3} \quad (8)$$

where Gr is the Grashoff number expressed as:

$$Gr = \frac{g\left(T_{abs} - T_C\right) e_a^3}{\upsilon^2 T_a} \quad (9)$$

$h_{r,C\text{-}sky}$ and $h_{r,C\text{-}abs}$ are the heat transfer coefficients by radiation, calculated respectively as:

$$h_{r,C\text{-}sky} = \varepsilon_C \ \sigma \ \left(T_C^2 + T_{sky}^2\right)\left(T_C + T_{sky}\right) \tag{10}$$

$$h_{r,C\text{-}abs} = \sigma \frac{\left(T_C^2 + T_{abs}^2\right)\left(T_C + T_{abs}\right)}{\frac{1}{\varepsilon_C} + \frac{1}{\varepsilon_{abs}} - 1} \tag{11}$$

where T_{sky} is the sky temperature, calculated as [13]:

$$T_{sky} = 0.0552 \ T_{amb}^{1.5} \tag{12}$$

2. Air Gap

$$\rho_a V_a C_a \frac{dT_a}{dt} = h_{cv,C\text{-}a} \ S_C\left(T_C - T_a\right) + h_{cv,abs\text{-}a} S_{abs}\left(T_{abs} - T_a\right) + U_{loss,e} S_{a,e}\left(T_{amb} - T_a\right) \tag{13}$$

$h_{cv,abs\text{-}a}$ is the heat transfer coefficient by convection between the absorber plate and the air gap, calculated using (7).

3. Absorber Plate

$$\begin{aligned} M_{abs} C_{abs} \frac{dT_{abs}}{dt} &= h_{r,C\text{-}abs} \ S_{abs}\left(T_C - T_{abs}\right) + h_{cv,abs\text{-}a} S_{abs}\left(T_a - T_{abs}\right) \\ &+ h_{cv,abs\text{-}f} \ S_{exch,f}\left(T_f - T_{abs}\right) + \left(U_{loss,b} S_{abs} + U_{loss,e} S_{abs,e}\right) \\ &.\left(T_{amb} - T_{abs}\right) + S_{abs} G \frac{\tau_C \alpha_{abs}}{1 - \phi_C\left(1 - \alpha_{abs}\right)} - Q_{abs\text{-}MCP}. \end{aligned} \tag{14}$$

$h_{cv,abs\text{-}f}$ is the convection heat exchange coefficient can be estimated using (7) and the correlation proposed by [14]:

$$Nu = 0.023 Re^{4/5} Pr^{0.4} \tag{15}$$

$U_{loss,b}$ and $U_{loss,e}$ are the bottom and the edge loss coefficients, calculated as:

$$U_{loss,b} = \frac{1}{\frac{e_{ins,b}}{\lambda_{ins,b}} + \frac{1}{h_{cv,wind}}} \ , \ U_{loss,e} = \frac{1}{\frac{e_{ins,e}}{\lambda_{ins,e}} + \frac{1}{h_{cv,wind}}} \tag{16}$$

where $Q_{abs\text{-}PCM}$ is the thermal exchange heat with the first PCM layer. During charging and discharging modes are expressed, respectively as:

$$Q_{abs\text{-}MCP} = - \ \lambda_{PCM,i} \ S_{PCM} \ \frac{\partial T_{PCM,i}}{\partial x} \Big|_{y=0} \tag{17}$$

$$Q_{abs\text{-}MCP} = \lambda_{PCM,i} \ S_{PCM} \ \frac{\partial T_{PCM,i}}{\partial x} \Big|_{y=0} \tag{18}$$

where i=sol when the PCM is in the solid phase and i=liq when the PCM is in the liquid phase.

4. Transfer Fluid

$$\rho_f C_f \frac{D_{int\text{-}Tube}}{4}\left(\frac{\partial T_f}{dt} + v_f \frac{\partial T_f}{dx}\right) = h_{cv,abs\text{-}f}\left(T_{abs} - T_f\right) \tag{19}$$

v_f is the transfer fluid velocity and $D_{int\text{-}Tube}$ is the tube diameter.

5. Phase Change Material

a. Charging Process

During the charging mode there are three steps: solid phase, solid-liquid phase and liquid phase.

- *Solid Phase ($T_{PCM} < T_{mel}$)*

The temperature distribution in the solid phase is governed by the conduction equation as:

$$\rho_{PCM,sol} C_{PCM,sol} \frac{\partial T_{PCM,sol}}{\partial t} = \lambda_{PCM,sol} \frac{\partial^2 T_{PCM,sol}}{\partial y^2} \tag{20}$$

The initial and boundary conditions are:

$$T_{PCM,sol}\left(y, \ t = 0\right) = T_{amb} \tag{21}$$

$$T_{PCM,sol}\left(y = 0, \ t\right) = T_{abs} \tag{22}$$

$$-\lambda_{PCM,sol} \frac{\partial T_{PCM,sol}}{\partial y}\Big|_{y = e_{PCM}} = U_{loss,b}\left(T_{PCM,sol}\left(y = e_{PCM}, \ t\right) - T_{amb}\right) \tag{23}$$

e_{PCM} is the PCM thickness.

- *Solid-Liquid Phase ($T_{PCM} = T_{mel}$)*

Fig. 2 shows the description of the heat transfer process in melting phase.

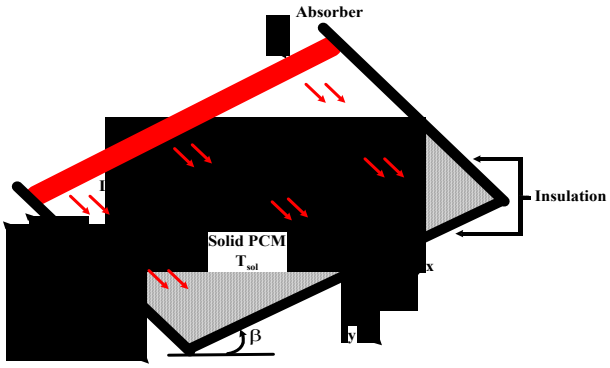

Fig. 2 Heat transfer process in the melting phase

Natural convection plays an important role in PCM melting. The importance of convection gradually increases as the molten region grows. Direct simulation of convection in PCM is complicated and needs too long computation time. In order to simplify the simulation, the convection effects are taken into account via the use of an effective conduction coefficient λ_{eff} expressed as [15], [16]:

$$\frac{\lambda_{PCM,eff}}{\lambda_{PCM,liq}} = a \ Ra^b \left(\frac{F_y}{L_{abs}}\right)^n \tag{24}$$

a, b, and n are constants which depend on the geometry and F_y and L_{abs} are the melt layer thickness and the absorber length, respectively.

The Rayleigh number Ra is expressed as:

$$Ra = \left[\frac{g\left(T_{abs} - T_{melt}\right)\rho_{PCM,liq}^{2} C_{PCM,liq} F_y^{3} \theta_{PCM}}{\mu_{PCM,liq}\lambda_{PCM,liq}} \right] \quad (25)$$

where θ is the expansion coefficient, μ is the dynamic viscosity, g is the gravity acceleration and T_{mel} is the melting temperature.

The temperatures distributions in the solid ($0<y<F_y(t)$) and the liquid ($F_y(t))<y<e_{PCM}$) phases are expressed by (20) and (26), respectively:

$$\rho_{PCM,liq} C_{PCM,liq} \frac{\partial T_{PCM,liq}}{\partial t} = \lambda_{PCM,eff} \frac{\partial^2 T_{PCM,liq}}{\partial y^2} \quad (26)$$

The analysis of heat transfer problems in melting process, called moving boundary problems in scientific literature, is especially complicated due to the fact that the solid-liquid boundary moves depending on the speed at which the latent heat is absorbed at the boundary, so that the position of the boundary is not known a priori and forms part of the solution. The Stephan condition, describes this process [17]:

$$\lambda_{PCM,sol} \frac{\partial T_{PCM,sol}}{\partial y}\bigg|_{y=F_y} - \lambda_{PCM,sol} \frac{\partial T_{PCM,liq}}{\partial y}\bigg|_{y=F_y} = \rho_{PCM,sol}\, Lv \frac{\partial F_y}{\partial t} \quad (27)$$

where Lv is the latent heat absorbed.

The boundary conditions for (26) are:

$$T_{PCM,liq}\left(y = F_y,\ t\right) = T_{PCM,sol}\left(y = F_y,\ t\right) = T_{mel} \quad (28)$$

$$T_{PCM,liq}\left(y = 0,\ t\right) = T_{abs} \quad (29)$$

- *Liquid Phase ($T_{PCM} > T_{mel}$)*

In this stage, the PCM is completely in liquid phase. The temperature distribution and the boundary conditions are expressed respectively by (26), (29) and (30).

$$-\lambda_{PCM,liq} \frac{\partial T_{PCM,liq}}{\partial y}\bigg|_{y=e_{PCM}} = U_{loss,b}\left(T_{PCM,liq}\left(y = e_{PCM},\ t\right) - T_{amb}\right) \quad (30)$$

b. Discharging Process

When the absorber attains the melt PCM temperature or when the rate of useful energy gain becomes less than the rate of the thermal losses, the PCM starts to solidify. For this operating mode, the thermal behavior and the boundary conditions of the PCM are governed by (5)-(16) and (18)-(30)

IV. Results and Discussion

The mathematical model obtained has been transposed into a Matlab computational program. The selected specification and design conditions of the integrated solar collector water heater are shown in Table I. The charging and discharging modes are analysed under different operating conditions. The parameters that maintained initially fixed are: the ambient temperature Tamb=31°C, the inlet water temperature Tf,in=31°C, the wind speed vwind=1.5 m/s and the mass flow rate ṁf=0.01 kg/s. The values adopted for the constants a, b, n in correlation (24) are 0.1, 0.25 and 0, respectively. The thermo physical properties of PCM used in this investigation are summarized in Table II. The results are presented only for the summer solstice (21st June).

TABLE I
Inputs Data for Simulation

Dimensions	1941 mm x 1027 mm x 88 mm	
Transparent cover	Glass without iron Thickness 3.2 mm Transmissivity (τ)=0.9 Emissivity=0.89	
Absorber	Copper Surface 1.87 m^2_Black selective absorptivity (α)=0.95 Emissivity=0.05	
Tubes	Copper Number of tubes13_Diameter=8.81mm	
Insulation	Bottom Glass wool Thickness=40 mm	Edge Polyester wool Thickness=28 mm

TABLE II
Thermo Physical Properties of PCM [18]

Properties	PCM
Melting temperature (°C)	42-44
Heat of fusion (J/kg)	$1.68\ 10^5$
Density[sol] (kg/m^3)	844
Density[liq] (kg/m^3)	760
Specific heat [sol] (J/kg.K)	2052
Specific heat [liq] (J/kg.K)	2411
Thermal conductivity [sol] (W/m.K)	0.4
Thermal conductivity [liq] (W/m.K)	0.15
Viscosity (Pa.s)	$4.9\ 10^{-3}$
Expansion coefficient (K^{-1})	$8.3\ 10^{-4}$

Climatic data using in this current investigation measured in Gabes (33°51N, 10°03E), Tunisia. Global solar radiation evolution in 21st June is shown in Fig. 3.

A. Distribution of PCM and Water Temperatures

Fig. 4 shows the temperature distribution for a 0.018 m of PCM versus time at different axial positions y=0 m, y=0.0053 m, y=0.0107 m, y=0.0162 m and y=0.018 m. The results present six steps, to complete the charging and discharging processes, namely: solid heating, melting, liquid heating, liquid cooling, solidification, and solid cooling. Firstly, the PCM temperature at each height is increased from the initial value (T_{PCM}=31°C) to the PCM melting point (T_{mel}=44°C) at almost the same speed and the thermal energy is stored as a sensible heat. After that, the PCM starts to melt and energy is stored as a latent heat. During the solid heating step, heat transfer is dominated by conduction while through the phase transition both conduction and natural convection are occurred. The importance of natural convection gradually increases as the melted PCM zone grows. When the PCM is fully melted, free convection within the PCM liquid and the

absorber plate becomes predominant, the PCM temperature at each height is increased again. The difference in temperature between the top and the bottom of PCM decreases, which is attributed to the enhancement of natural convection in liquid phase.

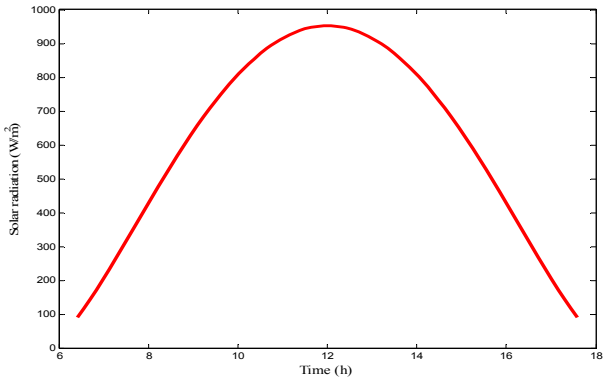

Fig. 3 Global solar radiation in 21st June

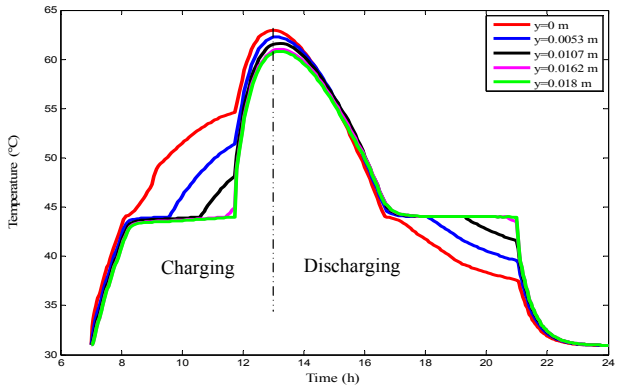

Fig. 4 Distributions of PCM temperature with time

During the cooling liquid stage, the PCM temperature decreases until its solidification point (T=44°C) due to the release of sensible heat stored in the PCM liquid. Fig. 4 also indicates a slight change in temperature curve order. Then, temperature remains constant until the end of solidification due to the release of the latent heat, the upper layer of PCM (y=0 m) solidifies firstly. Finally, another temperature drop is observed at the end of the discharging process. Natural convection is insignificant in the solidification phase and the heat transfer is governed only by conduction.

The melt fraction for 0.018 m of PCM during the charge and the discharge modes as a function of time is presented in Fig. 5. The PCM starts to melt at 8:06 am and the time to complete melting is 11:44 am. It is also seen that the melting process of all PCM has ended within 3 h and 38 min. The PCM solidification process starts at 16:39 pm to finish at 21:00 pm. Therefore, the time required to release the latent heat is approximately 4 h and 21 min. It is observed that the complete solidification time is longer than the melting time. This is because of the overall heat transfer coefficient which is low during solidification than the melting mode due to natural convection.

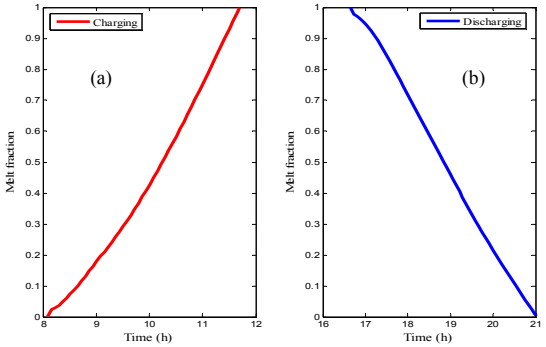

Fig. 5 Variation of melt fraction versus time during charging and discharging

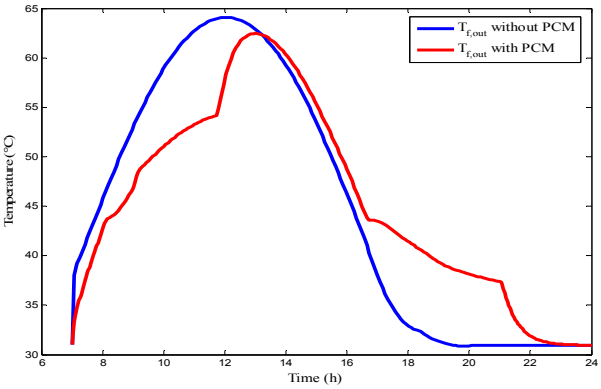

Fig. 6 Hourly variations of outlet water temperature without and with PCM

Fig. 6 shows the temperature variations of outlet water temperature without and with PCM as a function of time. For both cases, the temperatures increase with time until a maximum values and began to decrease after that. The highest water temperatures reached for the collector without and with a phase change material are approximately 64.08 and 62.48°C, respectively. This is can be explained by the rise of solar intensity in the morning and its decreasing in the afternoon. It is noticed also that the storage system slows down the increase and the decrease. This can be justified by the fact that for the case without PCM all absorbed solar radiations are used to heat the transfer fluid, contrary to the case where the PCM is used. In this last case, a portion of thermal energy is absorbed by the material in the charging process and this energy is released in the discharging process. As expected, the addition of PCM in solar systems causes a decrease in fluid temperature during charge and a rise during discharge.

B. Effect of Inlet Water Temperature

The effect of inlet water temperature on its outlet temperature is presented in Fig. 7. The curves are displayed for inlet temperature of 25, 30, 35, and 40°C. An increase in inlet temperature leads to a rise in outlet water temperature.

The highest temperatures reached are 54, 61.31, 66.76, and 71.50°C, respectively. It is observed that the addition of PCM causes a decrease in temperature during charge and a rise during discharge. The rise is most enhanced for higher inlet water temperature.

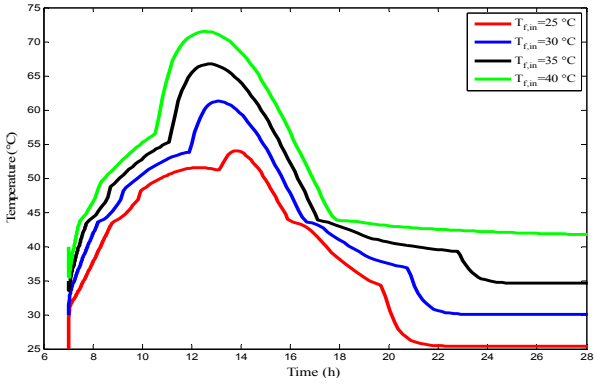

Fig. 7 Effect of inlet temperature on outlet water temperature

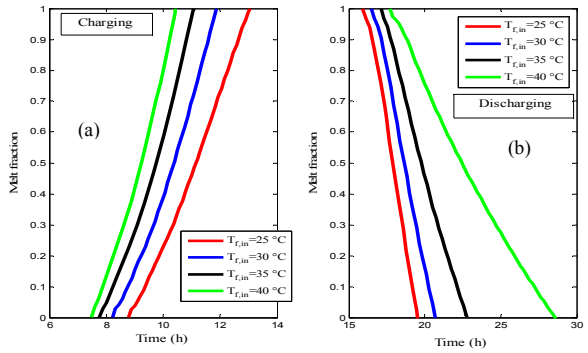

Fig. 8 Effect of inlet temperature on melt fraction during charging and discharging

The variation of the melt fraction for 0.018 m of PCM during charging and discharging modes versus time and for various inlet water temperatures is shown in Fig. 8. As expected, the higher the inlet water temperature is, the higher the melting speed is the shorter the melting time is and the longer the solidification time is. The times required to complete the melting process are 4.32 h, 3.68 h, 3.32 h and 3.07 h whereas the times to release the latent heat are approximately 3.78 h, 4.25 h, 5.64 h and 10.91 h when the inlet temperatures are 25, 30, 35 and 40°C, respectively.

C. Effect of Mass Flow Rate

The effect of the mass flow rate on the storage system performance is investigated in this section. The inlet water temperature and the PCM thickness are assumed to be 31°C and 0.018 m, respectively. Fig. 9 presents the outlet water temperature variation as a function of time. The results are displayed for water mass flow rates of 0.005, 0.008, 0.01 and 0.015 kg/s. The highest outlet fluid temperatures reached are 87.63, 69.70, 62.47and 49.77°C, respectively. The results show that the peak of outlet temperature increases with the decrease of flow rate. This is simply due to the fact that when the water flow rate rises, the amount of water to be heated with the same quantity of solar energy increases. The lower the mass flow rate is, the higher the water temperature during charging and discharging processes is.

The heat storage system requires a shorter time for the melting process; it spends a longer time to release the latent heat and has a higher fluid temperature at lower mass flow rate. Therefore, the smallest water mass flow rates are suitable for this solar system.

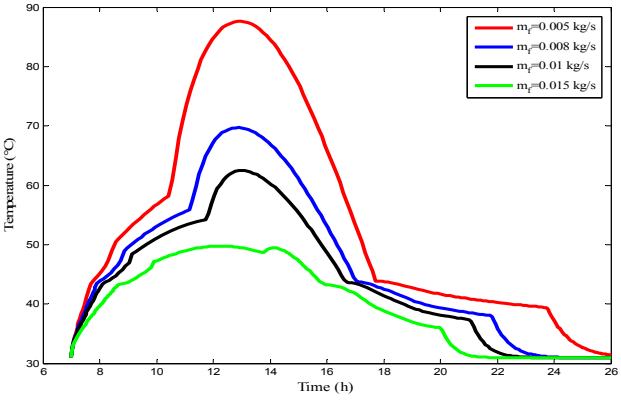

Fig. 9 Effect of mass flow rate on outlet water temperature

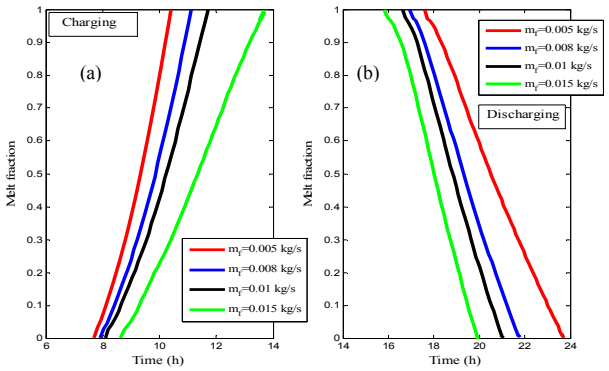

Fig. 10 Effect of mass flow rate on melt fraction during charging and discharging

Fig. 10 predicts the effect of the mass flow rate on the melt fraction. It can be observed that for the all mass flow rates the total melt fraction for the initial solid PCM height is 100%. The curves rise to complete solidification position early with the increase in the mass flow rate. Contrary to the case of melting process, the higher the mass flow rate is, the lower the melting speed is and the shorter the solidification time is. In fact, for mass flow rates of 0.005, 0.008, 0.01 and 0.015 kg/s the required melting times are 2.72 h, 3.25 h, 3.63 and 5.07 h, respectively whereas the solidification times are 6.06 h, 4.78 h, 4.38 h and 4.16 h. This may be due to the fact that when the mass flow rate increases the average absorber temperature drops resulting in a rise in the heat transfer between the absorber and the PCM during charging and discharging processes and therefore a rise and a decrease in the melting

and the solidification times, respectively. Numerical results show also that the rise in mass flow rate is not linear with the melting and solidification times. In other words, when the mass flow rate is doubled or tripled the melting and solidification times are smaller than twofold or threefold.

D.Effect of PCM Thickness

Fig. 11 presents the effect of PCM thicknesses on the outlet water temperature. The results are displayed for PCM height from 0 to 0.025 m. The higher temperatures reached are 64.08, 63.97, 63.90, 61.70 and 58.90 °C when the PCM thicknesses are 0, 0.005, 0.01, 0.02, and 0.025 m, respectively. As expected, the smaller the thickness is, the higher the maximum temperature reached is. Furthermore, a rise in PCM thickness leads to a decrease in temperature during charging and an increase during discharging. This is due that an increase in PCM thickness results in a rise in heat absorbed and released by PCM. It is observed also that the PCM thickness slows down the increase and the decrease.

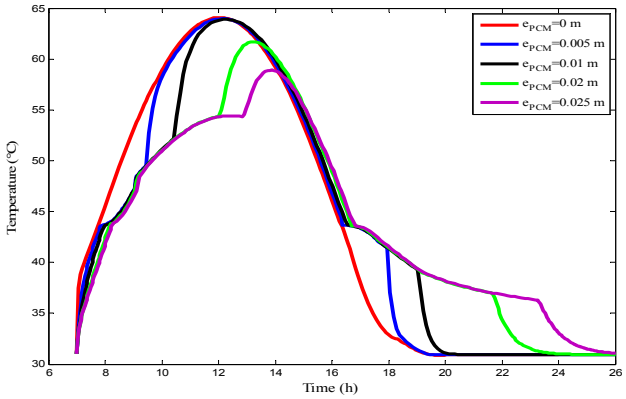

Fig. 11 Effect of PCM thicknesses on outlet water temperature

Fig. 12 shows the PCM melt fraction as a function of time during charging and discharging modes for different PCM thicknesses. The times required to complete the melting process are 1.6 h, 2.5 h, 3.88 h and 4.62 h while the solidification times are 1.6 h, 2.56 h, 5 h and 6.46 h when the PCM heights are 0.005, 0.01, 0.02 and 0.025 m, respectively. It is noticed that the times for complete melting and solidification are increased with the increase of PCM heights due to the heat transfer area between the PCM and the absorber plate. Furthermore, when the PCM thickness is doubled or tripled the melting time is much less than twofold or threefold. Thus, the rise in PCM height is not linear with the melting and the solidification times. It is also seen that the complete solidification time is longer than the melting time. This is because of the overall heat transfer coefficient which is low during solidification than the melting mode. Since the natural convection effect in the molten PCM of small thickness does not have significant influence on the charge rate, there is no significant difference between the complete melting and solidification time. Although, natural convection effect in the molten PCM is increased with the increasing of PCM height, consequently the difference between the complete melting and solidification times are rising.

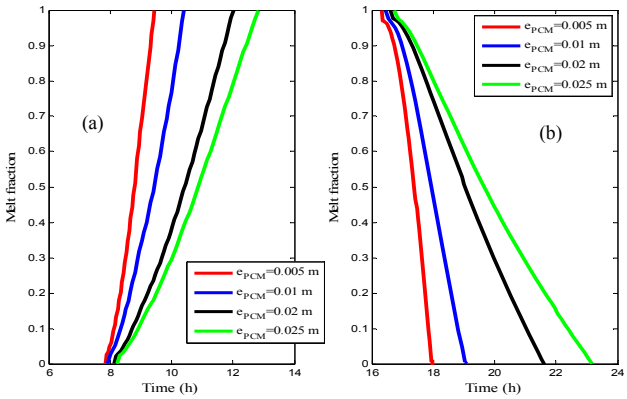

Fig. 12 Effect of PCM thicknesses on melt fraction during charging and discharging

V. Conclusion

A transient one dimensional theoretical model for thermal energy storage solar collector integrated with phase change material is developed to investigate the thermal performance of the system. The model is used to analyze the effect of inlet water temperature, mass flow rate and PCM thickness on the outlet water temperature and the melt fraction during charging and discharging processes. The important results obtained from this study are summarized as:

- The addition of PCM causes a decrease in temperature during charge and a rise during discharge. The rise is most enhanced for higher inlet water temperature, PCM thickness and for lower mass flow rate.
- The complete melting time is shorter than the solidification time due to the high heat transfer coefficient during melting. The natural convection effect in the molten PCM layer is increased with the increase of PCM thickness, thus the difference between the complete melting and solidification times is increased with the PCM height.
- The peak of outlet water temperature increases with the decrease of mass flow rate and PCM thickness and the rise of inlet water temperature.
- The higher the inlet water temperature is, the higher the melting speed is, the shorter the melting time is and the longer the solidification time is.
- The times needed to complete melting and solidification modes are not linear with the mass flow rate and the PCM thickness.

References

[1] A. K. Bhargava, "Solar water heater based on phase changing material," *Appl. Energy*, vol. 14, 1983, pp. 197-209.
[2] S. M. Shalaby, M. A. Bek, "Experimental of a novel indirect solar dryer implementing PCM as energy storage medium," *Energ. Convers. Manage.*, vol. 83, 2014, pp. 1-8.
[3] Y. Dutil, D. R. Rousse, N. Ben Salah, S. Lassue, L. Zalewski, "A review on phase-change materials: Mathematical modeling and simulations," *Renew. Sust. Energ. Rev.,* vol. 15, 2011, pp. 112-130.

[4] L. F. Cabeza, M. Ibanez, C. Sole, J. Roca, M. Nogues, "Experimentation with water tank including a PCM module," *Sol. Energy Mater. Solar Cells*, vol. 90, 2006, pp. 1273-1282.
[5] G. Serale, E. Fabrizio, M. Perino, "Design of a low-temperature solar heating system based on a slurry Phase Change Material (PCS)," *Energ. Build.*, vol. 106, 2015, pp. 44-58.
[6] G. N. Tiwari, S. N. Rai, S. Tram, M. Singh, "Performance prediction of PCM collection cum-storage water heater: quasi-steady state solution," *Energ. Convers. Manage.*, vol. 28, 1988, pp. 219-223.
[7] Y. Rabin, I. Bor-Niv, E. Korin, B. Mikic, "Integrated solar collector storage system based on a salt hydrate phase change material," *Sol. Energy*, vol. 55, 1995, pp. 435-444.
[8] A. Kürklù, A. Özmerzi, S. Bilgin, "Thermal performance of a water-phase change material solar collector," *Renewable Energy*, vol. 26, 2002, pp. 391-399.
[9] M. Chaabane, H. Mhiri, P. Bournot, "Thermal performance of an integrated collector storage solar water heater (ICSSWH) with phase change materials (PCM)," *Energ. Convers. Manage.*, vol. 78, 2014, pp. 897-903.
[10] S. Bouadila, M. Fteiti, M. M. Oueslati, A. Guizani, A. Farhat, "Enhancement of latent heat storage in a rectangular cavity: Solar water heater case study," *Energ. Convers. Manage*., vol. 78, 2014, pp. 904-912.
[11] S. M. A. Bekkouche, "Modélisation du comportement thermique de quelques dispositifs solaires," Thesis, University Abou-bakar Belkaid-Tlemcen, 2008.
[12] J. A. Duffie, W. A. Beckman, *Solar energy thermal process*, Wiley Interscience New York, 1974.
[13] K. Shiv, G. N. Tiwari, M. K. Gaur, "Development of empirical relation to evaluate the heat transfer coefficients and fractional energy in basin type hybrid (PV/T) active solar still," *Desalination*, vol. 250, 2010, pp. 214-221.
[14] F. P. Incropera, D. P. Dewitt, T. L. Bergman, V. S, Lavine, *Fundamentals of heat and mass transfer*, Six edition, 2006.
[15] A. Laouadi, M. Lacroix, "Thermal performance of a latent heat energy storage ventilated panel for electric load management," *Int. J. Heat Mass Transfer*, vol. 42, 1999, pp. 275-286.
[16] P. D. Silva, L. C. Gonçalves, L. Pires, "Transient behavior of latent-heat thermal energy store: numerical and numerical studies," *Appl. Energy*, vol. 73, 2002, pp. 83-98.
[17] A. B. Crowley, "Numerical solution of Stefan problems," *Int. J. Heat Mass Transfer*, vol. 21, 1978, pp. 215-219.
[18] L. Yang, X. Zhang, G. Xu, "Thermal performance of a storage packed bed using spherical capsules filled with PCM having different melting points," *Energ. Build.*, vol. 68, 2014, pp.639-646.